C. R. Physique 11 (2010) 87–95

Contents lists available at ScienceDirect

Comptes Rendus Physique

www.sciencedirect.com

Propagation and remote sensing / Propagation et télédétection

Modelling of the electromagnetic scattering by sea surfaces at grazing incidence. Application to HF surface wave radars

Modélisation la diffusion électromagnétique en incidence rasante par des surfaces océaniques. Application aux radars hautes fréquences à ondes de surface

Yaël Demarty [a,*], Laetitia Thirion-Lefevre [b], Vincent Gobin [c]

[a] *ONERA, centre de Palaiseau, DEMR, chemin de la Hunière, 91761 Palaiseau cedex, France*
[b] *SONDRA, Supélec, plateau de Moulon, 91190 Gif-sur-Yvette, France*
[c] *ONERA, centre de Toulouse, DEMR, 2, avenue Edouard-Belin, BP 4025, 31055 Toulouse cedex 4, France*

ARTICLE INFO

Article history:
Available online 21 February 2010

Keywords:
HF
Sea surface
Surface wave
Electromagnetic modelling
Electromagnetic scattering

Mots-clés :
ROS
Surface de mer
Onde de surface
Modélisation électromagnétique
Diffusion électromagnétique

ABSTRACT

The object of the study is to model the electromagnetic scattering by time-evolving sea surfaces illuminated by high frequency surface wave radars. A common way to simulate this case is to consider the scattering at grazing incidence. Recent studies have focused on so-called exact methods. As such methods are very time and memory consuming, it becomes important to implement techniques to reduce the calculation costs. Another important issue is to better understand the interactions between the electromagnetic waves and moving sea surfaces. We present in this article our simulator main characteristics and a comparison between simulated data and measurements.

RÉSUMÉ

L'objectif de cette étude est de modéliser la diffusion électromagnétique par des surfaces océaniques, lorsqu'elles sont éclairées par des radars hautes fréquences à ondes de surface. L'approche communément retenue est d'étudier la diffusion en incidence rasante. Des études récentes s'appuient sur des méthodes dites exactes. Comme de telles méthodes impliquent des temps de calculs et des volumes de données prohibitifs, il devient important d'implémenter des techniques permettant de réduire ces coûts. L'enjeu est également de comprendre les interactions entre l'onde électromagnétique et la surface océanique. Nous présentons dans cet article les principales caractéristiques de notre simulateur et une comparaison avec des mesures.

1. Introduction

The phenomenon of Bragg resonance in the Doppler spectrum at High Frequencies (HF) (3–30 MHz) was discovered by Crombie in 1955 [1]: the two principal peaks or lines (named first order spectrum) are the signature of the waves having a wavelength equal to half of the radar wavelength. In 1972, Barrick established an analytical model which provides an

* Corresponding author.
E-mail addresses: yael.demarty@isl.eu (Y. Demarty), laetitia.thirion@supelec.fr (L. Thirion-Lefevre), vincent.gobin@onera.fr (V. Gobin).

1631-0705/$ – see front matter
doi:10.1016/j.crhy.2010.01.003

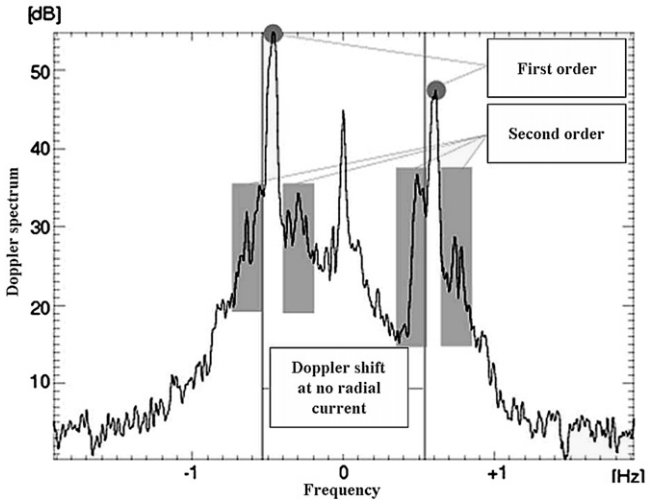

Fig. 1. Example of Doppler spectrum showing the first and the second order components as well as the Bragg line shift due to a marine current (illustration extracted from [8]).

Fig. 1. Exemple de spectre Doppler avec illustration du premier et du second ordre ainsi que du décalage des raies de Bragg dû à un courant marin (illustration tirée de [8]).

estimation of the first and the second order of a Doppler spectrum [2]. The two components of this spectrum are illustrated in Fig. 1.

The modelling of the Doppler spectra of sea surfaces in the HF band is of much interest for the oceanography community that initially looked for a tool of prediction and inversion. In fact, the idea is to extract from the Doppler spectrum the characteristics of the sea state such as the direction [3] and speed [4] of the wind, the wave height [5,6]. In parallel, some electromagnetic (EM) scattering models, more complete than Barrick's model were developed in order to remove the limitations of this latter [7,9]. For example, it does not allow to consider high sea states ($K.H_s > 4$ with K the radar wavenumber and H_s the significant wave height). Voronovich [10], Elfouhaily et al. [11,12], Bourlier et al. [13,14] in turn established various approximate models which are each one valid in a different frequency band, taking into account the multi-scale aspect of the sea surface, but showing their limits when considering grazing incidence and making assumptions on the sea roughness (for a summary of asymptotic methods the reader is referred to [15]). More recently, studies related to the development of models known as "exact modelling" have appeared (among them: Rino et al. in the HF band in 1991 [16], since 1996 Johnson et al. in the EHF and X bands [17,18], Toporkov and Brown in the C and X band starting from 1998 [19,20], Soriano and Saillard in the L band in 2003 [21]). These models are mainly based on the Method of the Moments (MoM) which can be solved by various algorithms (Fast Multipole Method (FMM), Method of Ordered Multiple Interactions (MOMI), Sparse Matrix Flat Surface Iterative Approach (SMFSIA), etc.).

In this article, we present our approach consisting in considering in the same time frequencies in the HF band, grazing angles and three-dimensional dynamic surfaces. These three aspects constitute critical points regarding both the numerical computation of the EM solution and the time and memory costs. In Section 2, we present our simulator and the methods used to overcome the difficulties mentioned above. The selected sea model is quite simple as it is based on the linear wave theory (cf. Section 2.2). Some validation results are then exposed in Section 3 as well as a comparison with the experiments carried out by ONERA (The French Aerospace Lab) in the Biscay bay (France) in 2007 in Section 4.

2. Presentation of the simulator

2.1. The electromagnetic model

The electromagnetic model uses a software developed by ONERA called Elsem3D (*Eléments finis pour la Simulation ElectroMagnétique* 3D) which implements the MoM. In order to accelerate the computing times, the resolution of the obtained matrix equation is performed using the combined integral representation of the electric field and the magnetic field (CFIE formulation). Moreover, to reduce the cost induced by the amount of data to store, the resolution of the problem is achieved by FMM. However, these last two choices require some adaptations of the studied surface. Indeed, the use of the CFIE formulation imposes that the simulated object is closed. This can be fulfilled by applying the image theory that leads to the study of the sea surface itself and its symmetrical image. These two elements constitute a closed geometry (see Fig. 2). To apply the image theory, we suppose that the simulated surface is perfectly conducting. This approximation is justified by the selected low frequencies and the grazing incidence (as shown in Fig. 3).

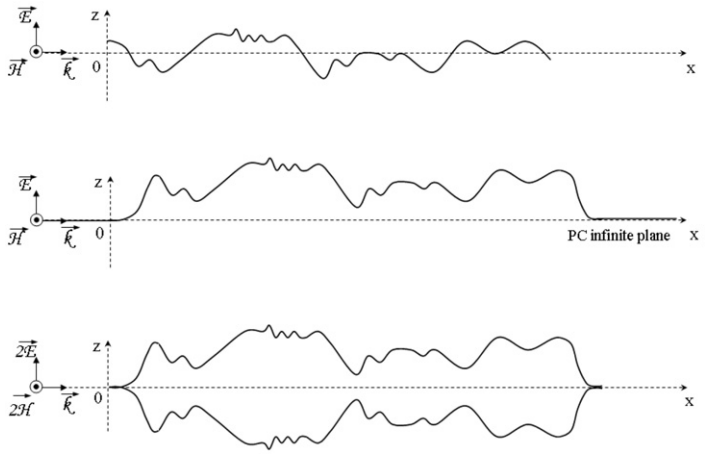

Fig. 2. The image theory applied to a source illuminating a rough surface enables to remove the infinite conducting plane, provided that an image source is added and that the geometry is symmetrical. In the top: initial surface with the incident wave. In the medium: surface translated along the z-axis, smoothed edges extended by an infinite conducting plane. In the bottom: case actually simulated with the symmetrical surface, the source and its superimposed image.

Fig. 2. La théorie des images appliquée à une source illuminant une surface rugueuse permet de retirer le plan conducteur infini, pourvu que l'on ajoute une source image et que la géométrie soit symétrisée. En haut : surface initiale avec l'onde incidente. Au milieu : surface rehaussée, bords lissés et prolongés par un plan conducteur infini. En bas : cas réellement simulé avec la surface symétrisée, la source et son image superposées.

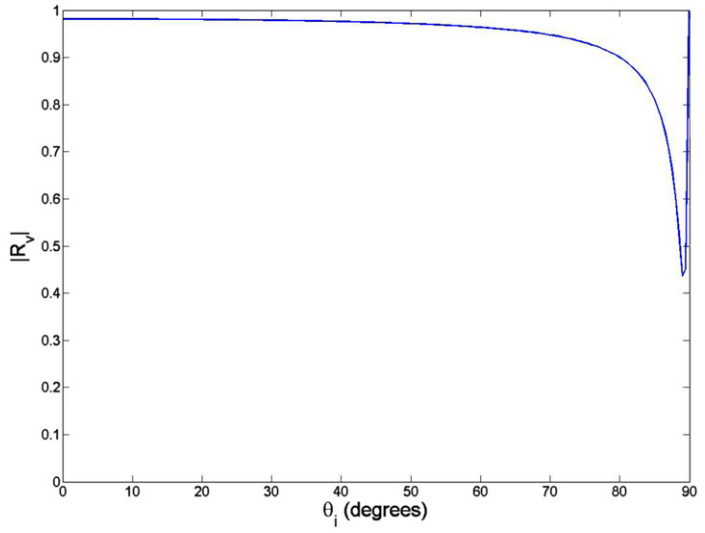

Fig. 3. The value of the reflection coefficient modulus in vertical polarization $|R_v|$ at high incident angles (grazing angles) and in HF is close to that of a perfectly conducting material. The frequency is 15 MHz, the permittivity and the conductivity of the sea are respectively $\epsilon_r = 80$ and $\sigma = 5$.

Fig. 3. La valeur du coefficient de réflexion en polarisation verticale aux forts angles d'incidence (angles rasants) et en bande HF est proche de celle d'un matériau parfaitement conducteur. La fréquence est de 15 MHz, la permittivité et la conductivité de la mer sont respectivement $\epsilon_r = 80$ et $\sigma = 5$.

In the end, our simulations can be summarized as the study of a closed, perfectly conducting object, illuminated by a source and the image source. Simulation times are highly reduced even if the number of unknowns has more than doubled as illustrated by Table 1.

Once the electromagnetic fields $\mathbf{E}(\mathbf{r}, t)$ calculated for each sampling time t_s composing the observation time T_{obs} and for a radar located at $\mathbf{r}$, it is possible to determine the Doppler spectrum of the sea surface:

$$S(f, \mathbf{r}) = \int_0^{T_{obs}} \mathbf{E}(\mathbf{r}, t) e^{-i2\pi ft}\, \mathrm{d}t \tag{1}$$

As our project focuses on the study of the modulus of this quantity, the term "Doppler spectrum" will refer to $|S(f, \mathbf{r})|^2$ all along this article. It should be noted that $\mathbf{E}(\mathbf{r}, t)$ is expressed in vertical polarization to simulate the behavior of HF-

Table 1
Illustration of the impact of the application of the image theory, the FMM and CFIE expression on the simulation duration.

Tableau 1
Illustration de l'impact de l'application de la théorie des images, de la FMM et de la formulation CFIE sur les temps de simulations.

Without the image theory	With the image theory
24 118 unknowns	48 596 unknowns
23.14 min	0.75 min

SWR and because the scene is perfectly conducting (the incident and scattered components of the EM field are in vertical polarization).

2.2. The sea model

The model of the sea that we chose relies on a linear formulation. This model is obviously not appropriate to accurately simulate the dynamic behavior of the sea. Nevertheless, it is an essential step to understand the involved physical phenomena. If one assumes that the sea can be described as a sum of N sinusoids, then the height h of this surface at each moment t_s and at any point $\mathbf{r}$ on this surface can be written as:

$$h(\mathbf{r}, t_s) = \sum_{n=1}^{N} A_n(\mathbf{k_n}) \cos(\mathbf{k_n} \cdot \mathbf{r} - \omega_n t_s + \varphi_n) \tag{2}$$

with $\mathbf{k_n}$ the wave vector of the nth sea wave, A_n its amplitude defined by the sea directional spectrum and $v_n = \omega_n / k_n$ the phase velocity. φ_n is here a random variable uniformly distributed in $[0, 2\pi]$. The sea spectrum selected for our study is also very simple as it is the JONSWAP (Joint North Sea Wave Project) spectrum [22] which was empirically determined from experiments in the North Sea. This spectrum is assumed to correctly model the gravity waves having a wavelength of around few meters and which propagate over large distances. These waves are in the same scale as the HF radar waves. The JONSWAP spectrum is multiplied by an angular function $D(\theta)$ which gives the main propagating direction θ_o to the waves. In our case [22]:

$$D(\theta) = \mathcal{N}(\mathfrak{s}) \cos\left(\frac{\theta - \theta_o}{2}\right)^{2\mathfrak{s}} \tag{3}$$

where $\mathfrak{s}$ is a spreading factor which depends on the wind speed and the sea state, $\mathcal{N}(\mathfrak{s})$ is a normalization function and θ_o the wind direction. If $\theta_o = 0$, the wind blows in the radar observation direction. In the case of gravity waves, in the deep water approximation and for a fully developed sea, the dispersion law is given by ${\omega_n}^2 = g k_n$ where g is the acceleration due to the gravity.

Finally, the dimensions of the scene were extracted from a statistical study of the surface roughness, and more precisely from the root-mean-square height H_{rms} and the correlation length L_c. The simulated surfaces are then $21L_c \times 21L_c$ large in order to be statistically representative of the sea state. Note that this does not necessarily ensure that the surface is sufficiently large to enable us to observe the EM surface wave propagation.

3. Some results of validation

Two types of simulations were performed to verify the correct behavior of our simulator. In the static case, the validation especially focused on the level backscattered first by simple objects (spheres, plane surfaces) and then by complex scenes (sea surfaces). The goal is in particular to check the good implementation of the image theory and the effect of the smoothed edges which were added. The dynamic validation consists in analyzing the Doppler spectra simulated in the case of propagating sinusoidal surfaces and then sea surfaces in movement. The objective is to determine under which conditions one can observe (or not) the Bragg phenomenon. This article only presents the dynamic aspect of the validation (for the static study see [23]).

3.1. From the sinusoidal surface to the sea

The EM wave reflected by a moving object of radial speed v presents a shift in frequency with respect to the incident wave called the Doppler frequency and defined by: $f_D = \frac{2v}{\Lambda}$ (Λ corresponds to the radar wavelength). In our case, it is necessary to take into account the frequency shift introduced by all the n gravity waves composing the surface. The velocity v_n of each wave is related to its spatial period λ_n and can be calculated by:

$$v_n = \sqrt{\frac{g\lambda_n}{2\pi}} \tag{4}$$

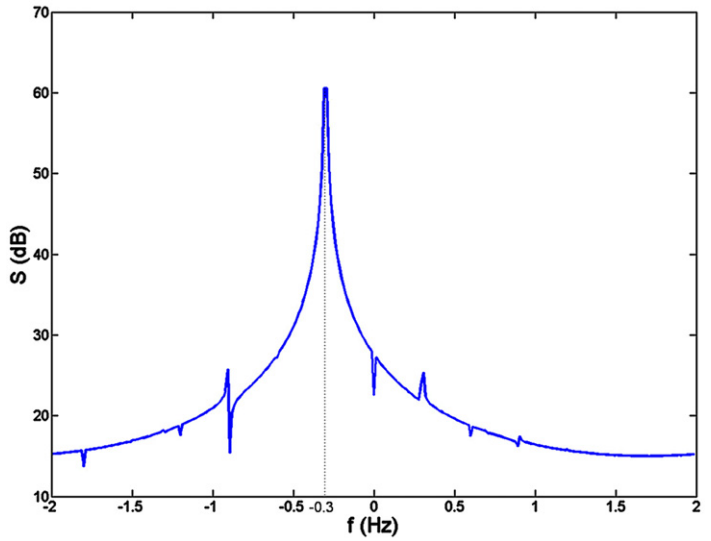

Fig. 4. Doppler spectrum of a sinusoidal surface defined by $h(t) = A \cdot \sin(2\pi/\lambda(x + vt))$ with $F = 15$ MHz, $v = 3$ m/s, $\lambda = 10$ m, $A = 1.8$ m, $T_{obs} = 50$ s, $t_s = 0.25$ s, $f_{B_{theo}} = -0.30$ Hz.

Fig. 4. Spectre Doppler d'une surface sinusoïdale.

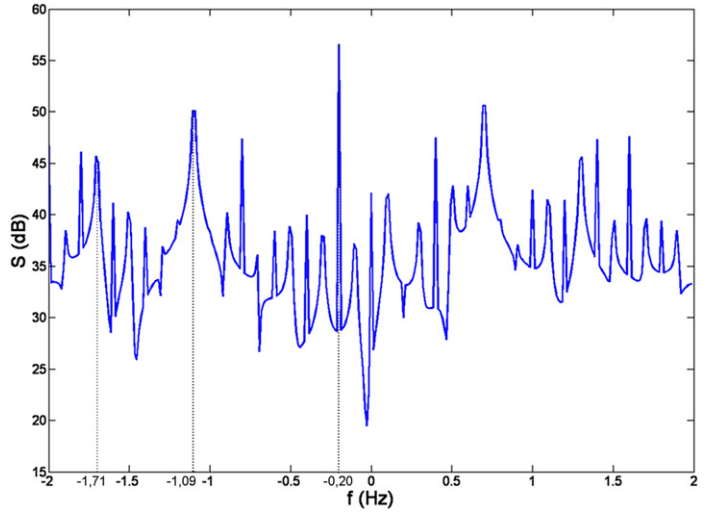

Fig. 5. Doppler spectrum of a sum of three sinusoidal surfaces $h(t) = \sum_{i=1}^{3} A_i \cdot \sin(2\pi/\lambda(x + v_i t))$ with $T_{obs} = 75$ s, $t_s = 0.25$ s, $\lambda = 10$ m, $v_1 = 2$ m/s, $A_1 = 1$ m, $v_2 = 11$ m/s, $A_2 = 0.5$ m, $v_3 = 17$ m/s, $A_3 = 0.2$ m leading to $f_{B1_{theo}} = -0.20$ Hz, $f_{B2_{theo}} = -1.1$ Hz and $f_{B3_{theo}} - 1.7$ Hz.

Fig. 5. Spectre Doppler d'une surface issue de la somme de trois sinusoïdes.

with $g = 9.81$ m/s. When the Bragg resonance occurs, i.e. when $\lambda_n = \Lambda/2$ then the Doppler frequency becomes:

$$f_{B_{theo}} = \sqrt{\frac{g}{\pi \Lambda}} \simeq 0.1\sqrt{F} \tag{5}$$

where F is the radar frequency in MHz. As one can see in Figs. 4, 5 and 6, the theoretical Bragg frequencies $f_{B_{theo}}$ are all retrieved in simulation, either in the case of the sinusoid (Fig. 4) or the sum of sinusoids (Fig. 5) or in the more complex case of a sea surface (Fig. 6). Some other signatures appear besides the Bragg line. They can be interpreted as harmonics of the Bragg frequency and the peak with a null Doppler shift is related to the fixed points of the simulated scene. The resonance phenomenon is even visible when the amplitude of the waves is set to a very low value (typically $A_3 = \Lambda/100$ in Fig. 5).

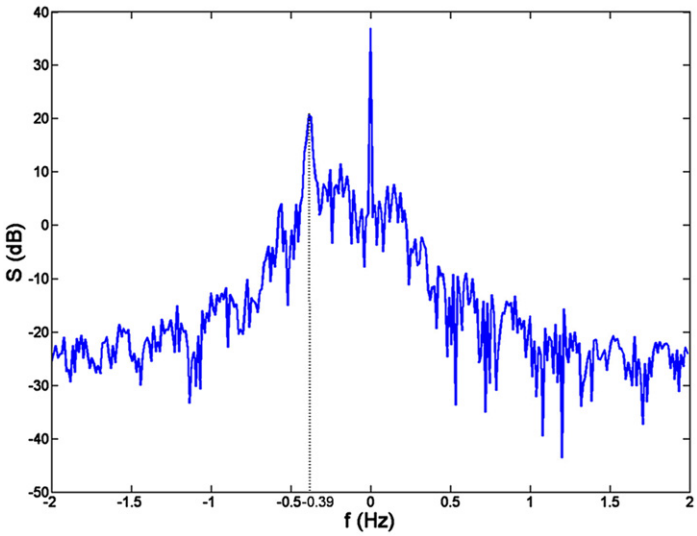

Fig. 6. Doppler spectrum of a sea surface propagating towards the radar with $T_{obs} = 75$ s, $t_s = 0.25$ s, the friction wind speed at the sea level $u_f = 19$ cm/s, $\theta_o = 10°$, $f_{B_{theo}} = +0.39$ Hz.

Fig. 6. Spectre Doppler d'une surface de mer se propageant vers le radar.

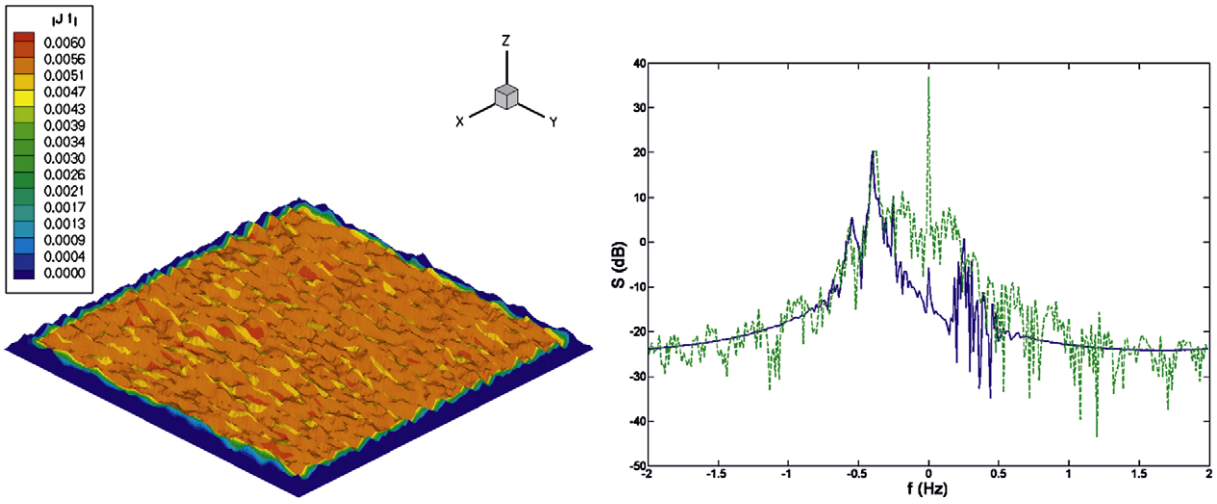

(a) (b)

Fig. 7. Visualization of the amplitude of the electrical current on a sea surface with cancellation of the currents on the smoothed edges (a). Comparison between a Doppler spectrum with (blue line) and without cancellation of the currents (green dashed line) (b).

Fig. 7. Visualisation de l'amplitude du courant électrique sur la surface avec annulation des courants sur les bords lissés (a). Comparaison entre un spectre Doppler avec (traits pleins bleus) ou sans (tirets verts) l'annulation des courants (b).

3.2. Effect of the edges

The influence of the addition of the smoothed edges on the backscattering coefficient of the sea surface is studied. They do not modify significantly this coefficient. However, as it is illustrated in Fig. 7(b), these smoothed edges have a strong impact on the Doppler spectrum. Indeed, the points at the limit of the simulated surface vary in height for each sampling time. This induces a modification of the slope of these edges. As a consequence, the edges oscillate with a velocity which does not correspond to a real sea wave velocity. This generates an artificial signature on the Doppler spectrum. In order to remove this artifact, the EM currents at the edges of the sea surface were systematically set to zero (as shown in Fig. 7(a)). The Doppler spectrum obtained is much less disturbed. The Doppler shifts and the harmonics induced by the components of the selected sea spectrum are now more clearly visible.

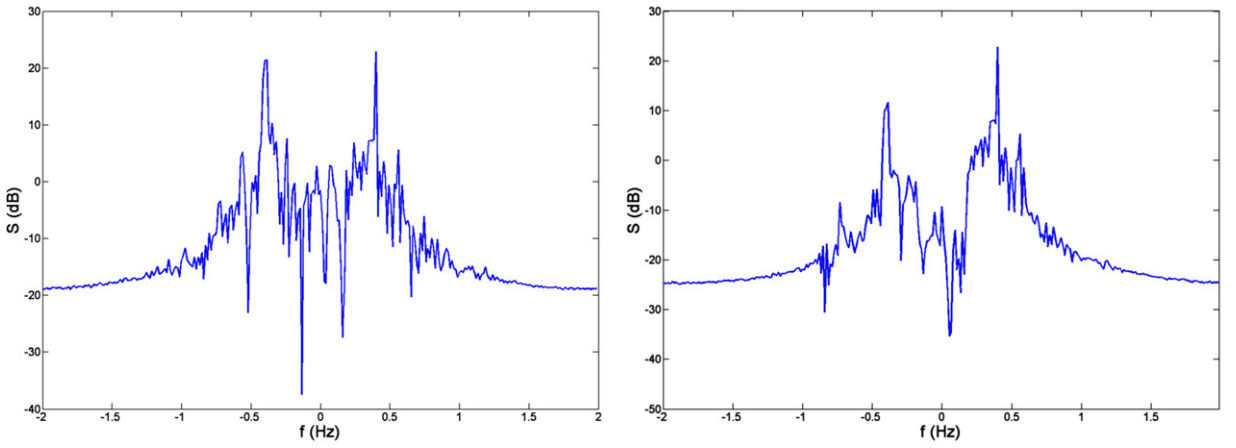

(a) (b)

Fig. 8. Doppler spectrum resulting from the addition to the sea surface of: (a) a wave system propagating in the opposite direction and (b) a noise propagating in opposite direction. The spectrum of the noise is constant with an amplitude equal to 1% of the maximum of the sea JONSWAP spectrum and without any main direction of propagation.

Fig. 8. Spectre Doppler résultant de l'addition à la surface de mer : (a) d'un système de vagues se propageant en sens opposé et (b) d'un bruit se propageant en sens opposé. Le spectre du bruit est constant, d'amplitude égale à 1% du maximum du spectre de mer de JONSWAP, sans direction de propagation privilégiée.

4. Simulation and experiment results

4.1. One or two Bragg lines?

The two Bragg lines (one of positive frequency, the other of negative frequency) underline the presence of two components of the spectrum linked to two movements of opposite directions: one going rather towards the radar, the other away from the radar. In our study, the selected sea spectrum (isotropic), associated to an angular function, provides a directional spectrum with a main propagation direction. In this case, only one Bragg line is observed. With our simulator, we identified two cases that can lead to the second line at the opposite frequency: the addition of a wave system propagating in the opposite direction or the addition of a noise to the sea surface. These two solutions are presented in Fig. 8. In the case of the noise (Fig. 8(b)), a constant sea spectrum with an amplitude much lower than the maximum value of the JONSWAP spectrum is considered. The main propagation direction of the noise is opposite to that of the sea waves. The angular function is set to 1 for all θ varying in $[0, \pi/2]$. This amounts to saying that the noise consists of multiple waves with low heights, propagating in all directions but in the opposite way to the sea waves. In this case, two lines of different amplitudes are visible.

The case where two identical sea surfaces (Fig. 8(a)), but with a propagation in opposite directions are superimposed, raises a problem of interpretation. On the coasts, it could correspond to the sea ebb and flow. In open sea, it implies the coexistence of two predominating winds blowing in opposite directions. However, this assumption does not have any physical sense. In addition, Doppler spectra confirm the presence of the two lines in the case of experiments carried out close to the coasts but what happens farther away? The measurements performed by ONERA show well an asymmetrical attenuation of the two peaks when going away from the coasts (see Fig. 9). The Bragg peak which persists corresponds to waves which move towards the radar.

4.2. Validation using the ONERA Biscay bay campaign

ONERA carried out during the summer 2007 a series of experiments in the Biscay bay with its new HFSWR (for details about the system see [24]). The sea state was well known thanks to the Gascogne buoy positioned at 310 km from the radar and equipped with a weather station (see [25] for more details). To be able to compare the simulated Doppler spectra with measurements, it is necessary to consider the differences between the simulation and the measurement. We have namely to take into account: the characteristics of the emitter and receiver (antenna gain, scattering pattern, amplifier gain, etc.), the configuration of the scene (dimension of the illuminated area, resolution cell dimension, propagation losses, etc.) and the different signal processing approaches. For some of these parameters it is quite easy to obtain an accurate value such as for the radar specifications or the normalization factor of the illuminated areas. Nevertheless, some others are not so straightforward to determine, like propagation losses. The corrections to apply to the simulated Doppler spectrum were provided by ONERA and are discussed in details in [23]. The first results (Fig. 9) show that the main peak of the Doppler spectrum is correctly located and that its amplitude is well modelled, provided that the comparison is done sufficiently far

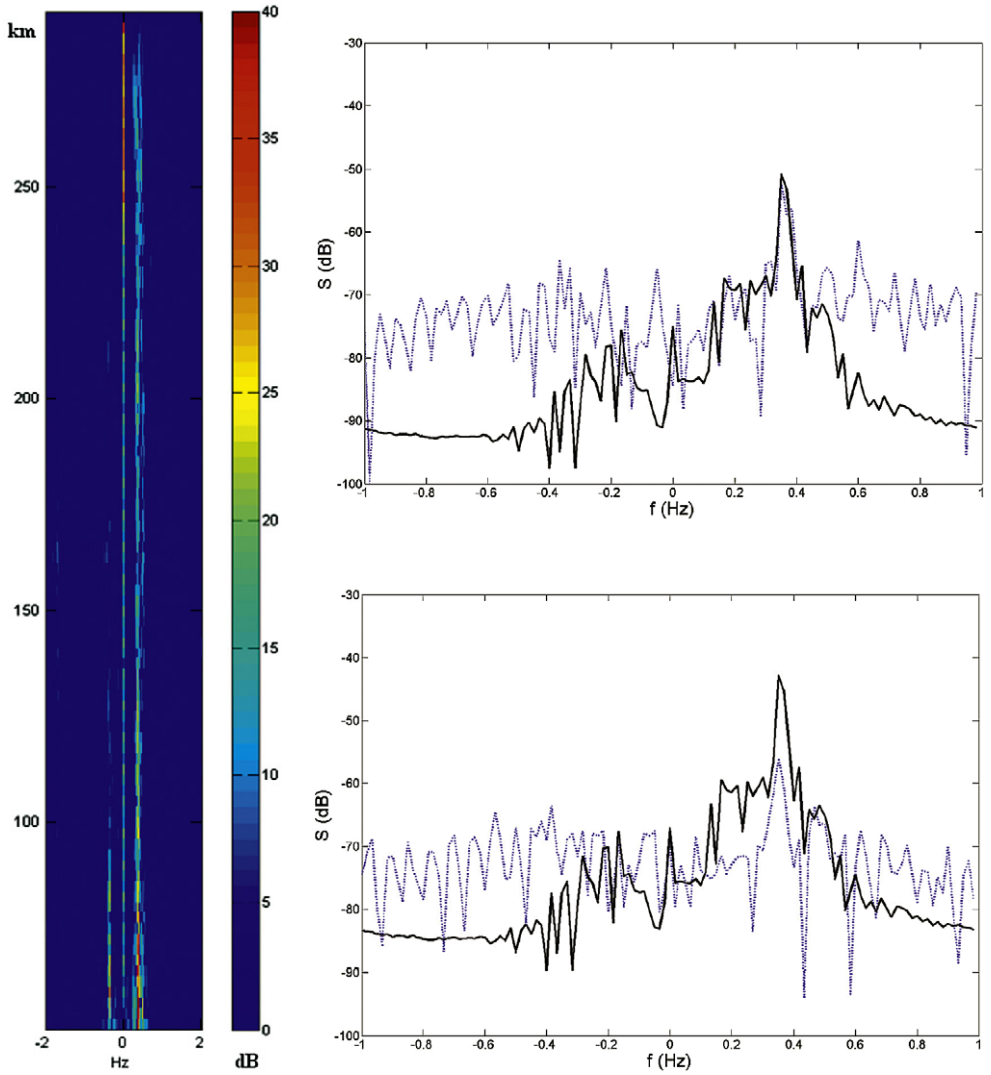

Fig. 9. Doppler-distance spectrum (**left**) measured with the ONERA HFSWR in the Biscay bay in Biscarrosse, Centre d'Essais des Landes, in July 2007, for distances from 50 to 300 km, $F = 12.5$ MHz. The sea state given by the Gascogne buoy was Beaufort 4–5, with a wind direction of West–South–West and a significant wave height $H_s = 1.7$ m. Comparisons between measured (blue dashed line) and simulated (black line) Doppler spectra at a distance from the coasts of 217 km (**top right**) and 195 km (**bottom right**) were performed with $\theta_o = 30°$, $H_s = 1.7$ m and a friction wind speed at the sea level of $u_f = 28$ cm/s.

Fig. 9. Spectre Doppler-distance (**gauche**) mesuré par l'ONERA avec un radar HFSWR dans la baie de Biscarrosse, au Centre d'Essais des Landes, en Juillet 2007, pour des distances de 50 à 300 km, $F = 12{,}5$ MHz. L'état de mer donné par la bouée Gascogne était Beaufort 4–5, avec une direction du vent Ouest–Sud–Ouest et une hauteur significative des vagues $H_s = 1{,}7$ m. Comparaisons entre des spectres Doppler mesurés (tirest bleus) et simulés (traits pleins noirs) à une distance des côtes de 217 km (**haut droit**) et de 195 km (**bas droit**), $\theta_o = 30°$, $H_s = 1{,}7$ m et la vitesse de friction du vent au niveau de la mer $u_f = 28$ cm/s.

from the coasts. As far as the level of the second order is concerned, there is a big difference between the two curves. Nevertheless, this point is not surprising as the second order observed on the Doppler spectrum results from the second EM and hydrodynamic order and the latter is not taken into account with the selected sea model. In addition, the simulations were carried out in the case of ideal conditions: without noise and in particular assuming that there was only one propagating wave system. Finally, the assumption was made that the sea conditions indicated by the Gascogne buoy were still correct closer to the coasts and that we could still suppose that the sea was fully developed. Taking into account these reserves, the results derived from these comparisons are very encouraging.

5. Conclusion

A simulator has been developed which relies on an electromagnetic modelling tool that enables it to take into account all the EM interactions. Our attention was particularly focused to accelerate the calculations in order to make the simulator

suitable for the analysis of sea Doppler spectra. The ocean model was selected as simple as possible, which was largely sufficient to test our tool as a first step. Validations were carried out and comparisons with ONERA measurements were achieved. The encouraging results that we obtained lead to the conclusion that this simulator is relevant for the study of ocean surfaces illuminated by an HFSWR. However, the sea modelling must be improved and it is particularly necessary to study the impact of the modelling of the non-linear components.

Acknowledgements

The authors are deeply grateful to the DEMR/RBF ONERA unit for carrying out the experiments and making possible the comparison with our simulations. They would also like to thank Jérome Simon (ONERA) for his help with Elsem3D and Bertrand Chapron (IFREMER) for his supportive ideas.

References

[1] Crombie, Doppler spectrum of sea echo at 13.56 mc/s, Nature 175 (1955) 681–682.
[2] Barrick, First-order theory and analysis of MF/HF/VHF scatter from the sea, IEEE Trans. Ant. Prop. 20 (1972) 2–10.
[3] Stewart, Barnum, Radio measurements of oceanic winds at long ranges: An evaluation, Radio Sci. 10 (10) (1975) 853–857.
[4] Huang, et al., HF radar wave and wind measurement over the Eastern China Sea, IEEE Trans. Geosc. Rem. Sens. 40 (2002) 1950–1955.
[5] Barrick, Directional sea spectrum determination using HF Doppler radar techniques, Radio Sci. 12 (1977) 415–424.
[6] Maresca, Georges, Measuring rms wave height and the scalar ocean wave spectrum with HF skywave radar, J. Geophys. Res. 85 (1980) 2759–2771.
[7] Wyatt, An evaluation of wave parameters measured using a single HF radar system, Can. J. Rem. Sens. 28 (2) (2002) 205–218.
[8] Gurgel, Essen, Schlick, An empirical method to derive ocean waves from second-order Bragg scattering: Prospects and limitations, IEEE J. Ocean Engrg. 31 (4) (2006) 804–811.
[9] Gurgel, Essen, Kingsley, HF radars: physical limitations and recent developments, Coastal Engineering 37 (1999) 201–218.
[10] Voronovich, Small-slope approximation in wave scattering by rough surfaces, Sov. Phys. JETP 62 (1985) 65–70.
[11] Elfouhaily, Chapron, A physically-based two scale electromagnetic model for backscatter from ocean-like surfaces, IGARSS 1 (1996) 600–602.
[12] Elfouhaily, Bourlier, Johnson, Two families of non-local scattering models and the weighted curvature approximation, Waves Random Media 14 (4) (2004) 563–580.
[13] Bourlier, Berginc, Saillard, Theoretical study of the Kirchhoff integral from two-dimensional randomly rough surface with shadowing effect: application on the backscattering coefficient for a perfectly conducting surface, Waves Random Media 11 (2) (2001) 91–118.
[14] Bourlier, Berginc, Saillard, Bistatic scattering coefficient from one- and two-dimensional random surfaces using the stationary phase and scalar approximation with shadowing effect – comparisons with experiments and application to the sea surface, Waves Random Media 11 (2) (2001) 119–147.
[15] Elfouhaily, Guerin, A critical survey of approximate scattering wave theories from random rough surfaces, Waves Random Media 14 (4) (2004) R1–R40.
[16] Rino, et al., Numerical simulation of backscatter from linear and nonlinear ocean surface realizations, Radio Sci. 26 (1991) 51–71.
[17] Johnson, et al., Backscattering enhancement of electromagnetic waves from two-dimensional perfectly conducting random rough surfaces: A comparison of Monte Carlo simulations with experimental data, IEEE Trans. Ant. Prop. 44 (1996) 748–756.
[18] Johnson, et al., A method of moments model for VHF propagation, IEEE Trans. Ant. Prop. 45 (1997) 115–125.
[19] Toporkov, Marchand, Brown, On the discretization of the integral equation describing scattering by rough conducting surfaces, IEEE Trans. Ant. Prop. 46 (1998) 150–161.
[20] Toporkov, Brown, Numerical simulation of scattering from time-varying, randomly rough surfaces, IEEE Trans. Geosc. Rem. Sens. 38 (2000) 1616–1625.
[21] Soriano, Saillard, Modelization of the scattering of electromagnetic waves from the ocean surface, PIER X (4) (2003) 102–128.
[22] Hasselmann, et al., Measurements of wind-wave growth and swell decay during the joint north sea wave project (JONSWAP), Deutsche Hydrographische Z. A (12) (1973).
[23] Demarty, Modélisation cohérente de la diffusion électromagnétique par des surfaces de mer tridimensionnelles en incidence rasante. Application aux radars HF à ondes de surface, Thèse de Doctorat, Université Pierre et Marie Curie, 2008.
[24] M. Menelle, G. Auffray, F. Jangal, Full digital high frequency surface wave radar: French trials in the Biscay Bay, IEEE RADAR (2008).
[25] National Oceanic and Atmospheric Administration (NOAA), National Data Buoy Center, http://www.ndbc.noaa.gov/station_page.php?station=62001.